

## THE TURBULENT BOUNDARY LAYER STRUCTURE OVER DIATOMACEOUS SLIME FOULING

**Elizabeth A. K. Murphy**

Department of Environmental Sciences  
University of Virginia  
Charlottesville, Virginia, 22903, USA  
eam6vf@virginia.edu

**Julio M. Barros**

Department of Mechanical Engineering  
United States Naval Academy  
Annapolis, Maryland, 21402, USA  
barros@usna.edu

**Michael P. Schultz**

Department of Naval Architecture and Ocean  
Engineering  
United States Naval Academy  
Annapolis, Maryland, 21402, USA  
mschultz@usna.edu

**Karen A. Flack**

Department of Mechanical Engineering  
United States Naval Academy  
Annapolis, Maryland, 21402, USA  
flack@usna.edu

**Cecily N. Steppe**

Department of Oceanography  
United States Naval Academy  
Annapolis, Maryland, 21402, USA  
natunewi@usna.edu

**Matthew A. Reidenbach**

Department of Environmental Sciences  
University of Virginia  
Charlottesville, Virginia, 22903 USA  
reidenbach@virginia.edu

### ABSTRACT

Biofilm fouling has a significant effect on ship performance. Here, the impact of biofilm fouling on boundary layer structure is investigated. Turbulent boundary layer measurements were performed over diatomaceous-slime-fouled plates using high resolution PIV. The mean velocity profile over biofilm shows the expected downward shift ( $\Delta U^+$ ), producing higher drag, and hence higher friction velocity. This increase in drag is seen in enhanced turbulent kinetic energy and Reynolds shear stress. Due to the complex nature of the biofilm's topography, the flow is heterogeneous in the streamwise direction when compared with smooth-wall flows.

### INTRODUCTION

Many biological surfaces are rough, and man-made surfaces, such as ship hulls, tidal turbine blades, and canals often become rough due to biological activity, such as the attachment and growth of organisms, also known as biofouling. This roughness impacts the performance of these engineered systems (Townsin 2003; Walker et al. 2013a; Walker et al. 2013b). Surface roughness due to biofouling on ship hulls has major economic consequences for shipping and Naval activities. For example, for mid-sized vessels alone, biofouling costs the U.S. Navy an estimated \$56 million per year due to increased fuel consumption and the costs of cleaning and painting the hull (Schultz et al. 2011). The primary biofouling community seen on Navy vessels is a biofilm, which is composed of bacterial or algal cells embedded in a viscoelastic extracellular polymeric substance (EPS) (Stoodley et al. 1999). The hydrodynamic regime a biofilm grows in, as well as the organismal makeup of a biofilm determines its physical structure. Different species have different cell surface properties (i.e. hydrophobicity or hydrophilicity), that

may influence how the structures interact with the flow within the viscous and turbulent boundary layer above the film (de Beer and Kühl 2001). Biofilm thicknesses range from micrometers to centimeters, and the structure of biofilms is highly heterogeneous, often composed of bulbous cell clusters between which are voids that permit fluid flow (de Beer et al. 1996). When grown under shear, biofilms form thin, flexible streamers that protrude from the surface (Taherzadeh et al. 2009). Eddies are shed off of the cell clusters, causing three-dimensional flapping of the streamers (Stoodley et al. 1998). Biofilms found on ship hulls are often primarily composed of diatoms, and are referred to as diatomaceous slimes (Schultz et al. 2015). Fouling-release and antifouling hull coatings can be ineffective at preventing diatomaceous slime fouling (Molino and Wetherbee 2008). These slimes are also common on marine sediments, where they stabilize the sediment and may alter transport between porewater and the water column (Tolhurst et al. 2008). Though biofilms typically have low vertical relief and the roughness elements are compliant, biofilm fouling induces a steep drag penalty on fouled surfaces, increasing the skin friction on a plate by up to 70% of that of a smooth surface (Schultz et al. 2015). Field and laboratory trials indicate that slime on ship hulls significantly increases the resistance and power requirements of the vessel (Schultz 2007; Haslbeck and Bohlander 1992).

In most cases, studies of the effects of roughness on the turbulent boundary layer focus on rigid roughness elements, often with regular spacing (Krogstad and Antonia 1999; Flack et al. 2005; Flack and Schultz 2010). However, in biological systems, compliance and irregularity are the norm. Direct measurements show that biofilms increase skin friction on fouled surfaces, and analysis of the mean velocity profile shows that the effective roughness ( $k_s$ ) of a biofilm is greater than the physical height of

Table 1. Roughness parameters of the biofilm-fouled plate and the smooth plate.  $\delta^+$  is the friction Reynold number.

	$U_e$ ( $m s^{-1}$ )	$\delta$ ( $mm$ )	$Re_\tau = \delta^+ = \delta U_\tau / \nu$	$U_\tau$ ( $m s^{-1}$ )	$\Delta U^+$	$k_s^+$	$k_s$ ( $mm$ )	$C_f$	$\ell_v$ ( $m$ )
Smooth	1.2	33.5	$1.6 \times 10^3$	0.046	-	-	-	$2.8 \times 10^{-3}$	$2.1 \times 10^{-5}$
Biofilm	1.1	30.0	$2.5 \times 10^3$	0.076	12.8	735.8	8.8	$9.0 \times 10^{-3}$	$1.2 \times 10^{-5}$

the biofilm itself (Walker et al. 2013b). However, under some wall boundary conditions a compliant surface can decrease skin friction due to turbulence by lessening the intensity of turbulence near the wall and reducing the amount of energy carried in streamwise vortices (Xu et al. 2003). Some studies of biofilms and other types of algae growth on already-rough surfaces such as coral reefs or pebbles show a reduction of surface roughness as well as a decrease in bed shear stresses compared to the bare roughness elements because the biofilm growth effectively smooths out the surface (Graba et al. 2010; Nikora et al. 2002; Stocking et al. 2016). It is generally accepted that the effects of roughness on the mean velocity profile in the boundary layer, at high Reynolds numbers relevant to ships, are limited to the inner portion of the boundary layer when the height of the roughness elements are significantly smaller than the boundary layer thickness (Castro 2007, Flack and Schultz 2014, Wu and Christensen 2007). This is referred to as outer layer similarity, where that the outer layer of the turbulent boundary layer over rough and smooth walls is unaffected by the surface roughness (when flow characteristics are normalized by the wall shear velocity). This assumption of outer layer similarity holds for biofilms (Walker et al. 2013b) and forms the basis of scaling techniques that aim to model the effects of surface roughness on vessel performance (Schultz 2007). Different types of roughness can have similar effects on the mean velocity profile (e.g. mesh and rods (Krogstad and Antonia 1999)), but different effects on turbulence generation and turbulent stresses; i.e. roughness alters the structure of the turbulence itself within the boundary layer, altering the size and coherence of vortices and the generation of turbulence at the wall (Volino et al. 2009; Volino et al. 2011, Wu and Christensen 2010, Mejia-Alvarez and Christensen 2011). However, little is known about how compliant roughness alters this turbulence structure.

Detailed planar flow measurements are presented over a large biofilm-fouled plate. In order to assess both the average velocity field over a biofilm as well as the heterogeneous nature of turbulence parameters over a natural living surface, high resolution 2-D particle image velocimetry (PIV) was used on the boundary layer in moderate Reynolds number flow. The results presented are for a uniformly-fouled plate with relatively thick biofilm fouling. Therefore, the methodology used, where both the velocity field throughout the boundary layer, and the spatially-resolved generation of turbulent and shear stresses are measured, provides insights into the mechanisms of the effects of biofilm on boundary layer flow. Given that biofilms can show a large increase in skin friction despite a small physical roughness height, this study examines the spatially explicit effects of a biofilm on the shear velocity, turbulent kinetic energy, instantaneous momentum transport, rotational motion, and coherent structures within the turbulent boundary layer.

## MATERIALS AND METHODS

### Biofilm and Facilities

A dynamic slime exposure facility, described in Schultz et al. 2015, was used to grow biofilm on large (200 mm x 1.52 m) acrylic plates affixed to the outside of a rotating drum submerged in brackish water with a salinity of 18 ppt. The drum rotates at 60 rpm, creating a peripheral velocity of  $1.9 \text{ ms}^{-1}$ , so that biofilm growth occurred under shear. The biofilm consisted of four genera of diatoms (*Amphora*, *Achnanthes*, *Entomoneis* and *Navicula*) that are commonly found on ships, and are also found on antifouling and fouling-release coatings that have been exposed to the marine environment under dynamic conditions (Schultz et al. 2015). The fouled plate tested was exposed in the dynamic slime facility for 10 weeks and had a uniform layer of biofilm that averaged  $1.7 \pm 0.5 \text{ mm}$  thick with a mean peak-to-trough distance of 0.5 mm.

Testing was performed in a recirculating tunnel facility in the United States Naval Academy Hydromechanics Laboratory. The flow enters the test section through several flow-conditioning devices: a contraction, mesh screens and a honeycomb flow straightener. The freestream turbulence in this facility is less than 0.5% (Volino et al. 2007). The test section of the tunnel is 0.2 m x 0.1 m, with a length of 2 m. The adjustable top wall of the tunnel was set to provide a zero-pressure gradient flow during testing. The free stream velocity was  $1.1 \text{ ms}^{-1}$ .

Particle image velocimetry (PIV) was used to capture the flow field in the streamwise - wall-normal ( $x - y$ ) plane. The system consisted of one  $6.6k \times 4.4k$  pixels 12 bit frame straddle CCD camera (TSI 29MP) coupled with a 190 mJ per pulse, dual-cavity pulsed Nd:YAG laser (Quantel). A 0.3 mm thick laser lightsheet was formed by a spherical-cylindrical lens configuration. The flow was seeded with  $2 \mu\text{m}$  silver coated glass-sphere particles, and all measurements were performed  $\sim 1.22 \text{ m}$  downstream of the boundary layer trip, and  $\sim 0.42 \text{ m}$  downstream of the leading edge of the fouled plate.

Image pairs were processed using a recursive Nyquist grid with 50% overlap ending in a  $32^2$  pixel window, resulting in a velocity resolution of  $176 \mu\text{m}$  and a field of view of  $72 \times 42 \text{ mm}$  ( $2.4\delta \times 1.4\delta$ ). Vectors statistically very different from their neighbours were removed and replaced with interpolated vectors. More details of PIV processing are given in Barros et al. 2016.

Smooth wall boundary layer data is used for comparison in this study. Data were taken in the same facilities as the biofilm data over a smooth acrylic plate. Spatially explicit data are from the PIV analysis as described above, with a  $157.27 \times 51.47 \text{ mm}$  window. The spatial resolution of the smooth wall PIV vector data is  $144 \mu\text{m}^2$ . Additionally, a smooth wall mean velocity profile was taken using Laser Doppler Velocimetry (LDV) at the same PIV measurement location for comparison purpose. The LDV setup was similar to that described in Schultz and Flack 2007.

Flow parameters for the smooth wall and slime-fouled wall are given in Table 1. The boundary layer thickness,  $\delta$ , was measured from 0.5 mm below the height of the tallest point of the biofilm.

### Mean Velocity Profile Analysis

The log-law equation for flow over a smooth wall,

$$U^+ = \frac{1}{\kappa} \ln(y^+) + C \quad (1)$$

describes the mean boundary layer velocity profile in the log region above the bed. Here, the + superscript indicates that the term is normalized by inner units ( $U_\tau$  and  $\frac{y}{U_\tau}$ ). Both  $C$  and  $\kappa$  are empirically derived universal constants.  $C$  is the log-law intercept for the smooth wall, here set to 5.2, and  $\kappa$  is the von Kármán constant, 0.41 (Flack et al. 2005). The structure of flow over a rough wall is altered, with the addition of a wall datum offset ( $\epsilon$ ) and the roughness function ( $\Delta U^+$ ), so that the flow in the log-region of a rough wall boundary layer is described by

$$U^+ = \frac{1}{\kappa} \ln(y + \epsilon)^+ + C - \Delta U^+ \quad (2)$$

where  $\Delta U^+$  results in a downward shift of the velocity profile, and  $\epsilon$  is the vertical displacement of the virtual origin. The addition of these two variables complicates finding the shear velocity,  $U_\tau$ . Typically, an iterative procedure is used to adjust the values of  $U_\tau$  and  $\epsilon$  until the slope matches that of the smooth wall (Perry and Li 1990). However, for our biofilm flows the log-layer appears to be too thin for this method to be effective. This may be due to interference of flow visualization very close to the wall by the biofilm or by the relatively modest Reynolds numbers of the tests. However, the boundary layer velocity profile can also be described in the velocity defect form,

$$U_e^+ - U^+ = -\frac{1}{\kappa} \ln\left(\frac{y+\epsilon}{\delta}\right) + \frac{2\pi}{\kappa} w(y/\delta) \quad (3)$$

where  $\frac{2\pi}{\kappa} w(y/\delta)$  is the wake function, which describes the behavior of the flow in the outer layer. The wake function should be similar between the biofilm and the smooth wall, because the height of the biofilm is small compared to the thickness of the boundary layer (Tani 1987; Jimenez 2004), and measurements by Walker 2013b over a freshwater biofilm find outer layer similarity. Therefore, velocity defect similarity between the biofilmed surface and a smooth wall was assumed (Flack et al. 2005, Castro 2007), using an iterative goodness-of-fit maximization scheme between the biofilm velocity defect profile and the smooth wall velocity defect profile to calculate  $U_\tau$  and  $\epsilon$  over the biofilmed surface.  $\Delta U^+$  was calculated by finding the value that resulted in the best match between the log and wake regions of the biofilm and smooth wall mean velocity profiles plotted in inner units. The initial origin was set at 0.5 mm below the maximum height of the biofilm across the frame.

## RESULTS

### Mean Velocity Profile Analysis

Figure 1 shows the mean velocity profile over the biofilm normalized using inner units (left panel) and outer units in velocity defect form (right panel), with the smooth wall profile from both PIV and LDV for comparison. The turbulent boundary layer over the biofilm appeared to exhibit a standard mean velocity profile, with a log-law region and the expected downward shift ( $\Delta U^+$ ) found in rough-wall flows (Fig.1 left panel).

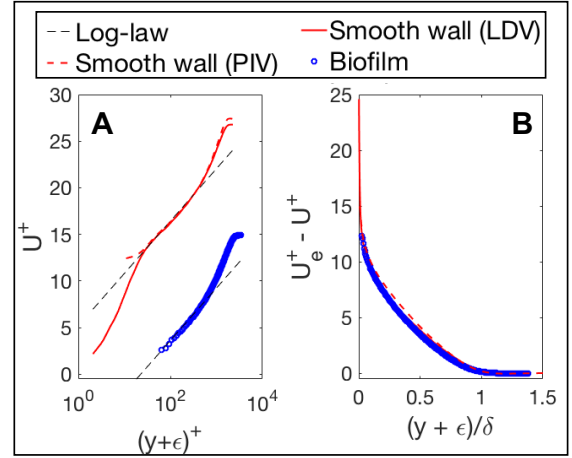


Figure 1. Average streamwise velocity profile over the biofilm and smooth wall in A) inner units and B) velocity defect form.

From table 1, the roughness function is  $\Delta U^+ = 12.8$  which indicates the flow is in the fully-rough regime. This yields an equivalent sand-grain roughness height,  $k_s$ , of 8.8 mm. This means that the biofilm destroys the viscous sublayer, and the roughness effect on the mean flow is large. However, when the biofilm mean velocity profile is presented in the defect form, it can be seen that a good collapse with the smooth-wall is observed.

Figure 2 shows the streamwise average of the Reynolds stress profiles, normalized in inner units. Additionally, the local profiles at each streamwise location are shown to highlight the heterogeneities that the biofilm bed introduces in the roughness sublayer. The peak streamwise Reynolds stress over the biofilm is shifted away from the bed as compared with the smooth wall. This is similarly seen over non-uniform biofilm fouling (Walker et al., 2013), and is due to the relative increase of friction forces due to drag on the roughness elements and resulting relative decrease in viscous forces. The Reynolds shear stress has a sharper peak than the smooth wall, and appears slightly elevated compared to the smooth wall, however the local profiles exhibit a range of peak values. The streamwise mean Reynolds stress profiles are at the higher end of the range of the local profiles, due to the mean shear velocity, calculated from the streamwise average velocity profile, being slightly lower than most of the local shear velocities. It is worth pointing out that the local profiles display a collapse of the Reynolds stresses in the outer

layer, when compared with the smooth-wall Reynolds stresses profiles. The smooth wall data is from PIV.

### Spatially explicit mean flow analysis

The 2D turbulent kinetic energy ( $tke = \frac{1}{2}(u'^2 + v'^2)$ ), normalized by the freestream velocity, is enhanced over the biofilm (Fig. 3).

Turbulent kinetic energy ( $tke$ ) in the flow over the biofilm exhibited spatial heterogeneity compared to that over the smooth wall, and the core of  $tke$  ( $y/\delta > 0.1$  and  $y/\delta < 0.4$ ) is more than 4 times greater than that of the smooth-wall case. Similar results are also seen for the  $RSS$  (Fig. 4), where the core of the Reynolds shear stress is enhanced and heterogeneous in the streamwise direction.

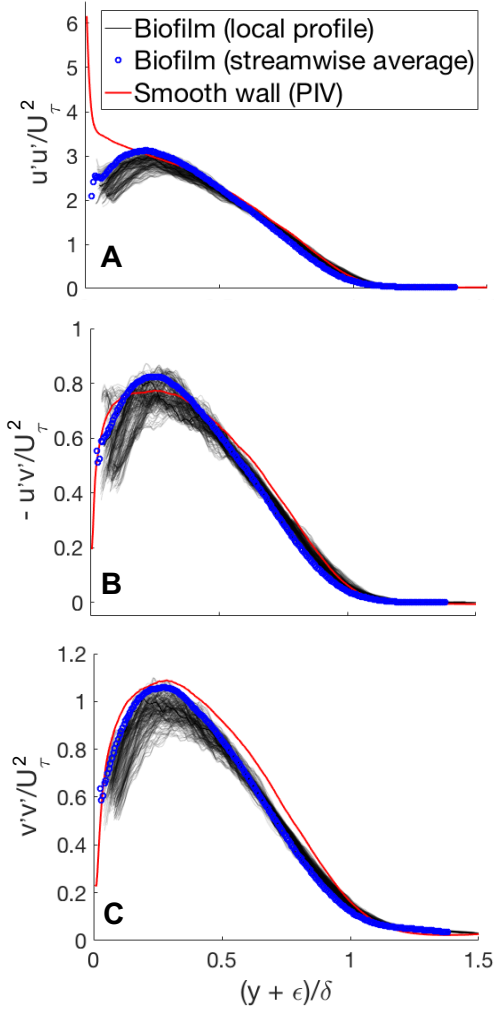


Figure 2. Average streamwise Reynolds stresses over the biofilm and smooth wall. The local values of the Reynolds stresses above the biofilm are also presented. A)  $u'^2$ ; B)  $-u'v'^2$ ; C)  $v'^2$

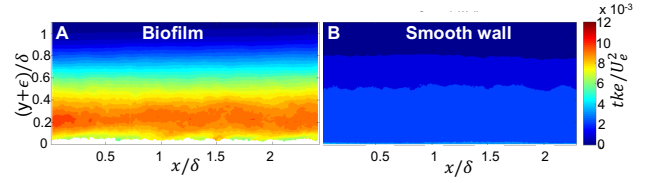


Figure 3. 2D turbulent kinetic energy ( $tke$ ) normalized by the free stream velocity ( $U_e^2$ ) over the biofilm (A) and over the smooth wall (B).

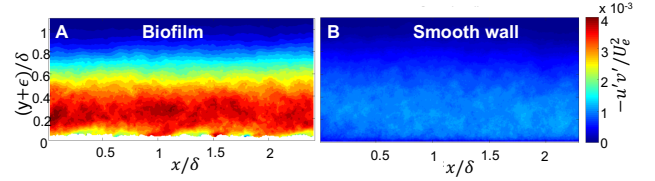


Figure 4. Reynolds shear stress ( $RSS$ ), normalized by  $U_e^2$  over the biofilm (A) and the smooth wall (B).

The production of  $tke$  ( $P = -u'v' \frac{\partial u}{\partial y}$ ) appears to be spatially heterogeneous (Fig. 5), and also appears to be strongest on the downstream edges of roughness elements in the biofilm layer. These near bed hotspots of  $tke$  production are likely indicative of increased turbulent transport and vertical mass and momentum transport (Reidenbach et al. 2010), suggesting that enhancement of access to nutrients due to turbulence is locally variable.

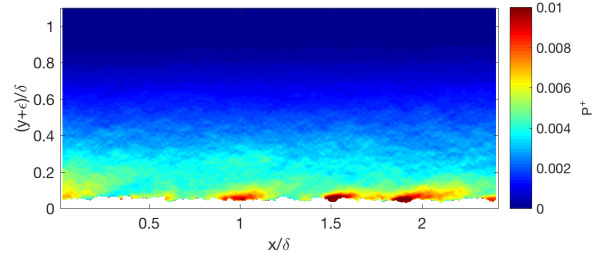


Figure 5. Production of  $tke$  ( $P$ ), normalized by  $U_e^3$ .

### Spatial Coherence Analysis

Coherent structures in the turbulent flow were assessed using three methods: two-point correlation, quadrant analysis and the probability density function of the instantaneous  $RSS$ .

The inhomogeneous two-point correlation in the streamwise-wall normal plane is given as

$$\rho_{u_i u_j} = \frac{u_i(x_{ref}, y_{ref}) u_j(x_{ref} + \Delta x, y_{ref} + \Delta y)}{\sigma_{u_i}(x_{ref}, y_{ref}) \sigma_{u_j}(x_{ref} + \Delta x, y_{ref} + \Delta y)} \quad (5)$$

where  $\rho_{u_i u_j}$  is the two-point correlation normalized by the standard deviation of the local velocity and the reference velocity, and  $x_{ref}$  and  $y_{ref}$  denote the reference location. Here we used  $y_{ref} = 0.3\delta$  and  $x_0$  was taken as the middle of the frame (Fig. 6). Focusing on the streamwise correlation, we see that there is little qualitative difference between the smooth wall and the biofilm flows. In both cases,  $\rho_{u_i u_i}$  is elongated in the streamwise direction

and is characterized by similar inclinations of the correlation. The angle of inclination of the two-point correlation of  $u$ , indicated by the black line in Fig. 6C & 6D, is an indication of the angle coherent structures that are shed from the wall (Volino et al. 2007). The angle of inclination of  $\rho_{uu}$  is  $12.6^\circ$  for the smooth wall and  $16.3^\circ$  for the biofilm wall, and was calculated by finding the point on each contour line that is furthest from the reference point and fitting a line through them. The inclination angle indicates that vortical structures in the flow move coherently away from the wall similarly to those above the smooth wall. Coherent vortical structures are important in the transport of turbulence in the boundary layer, especially the ejection of low-momentum fluid from near the bed into the outer layers (Moin and Kim 1985). The similarity in shape and angle of the streamwise correlation over the rough biofilm surface and the smooth wall has been seen over other types of 3D roughness, both irregular (Wu and Christensen 2010) and regular (Volino et al. 2007), though these studies also find a small decrease in the streamwise length of the correlation. Additionally, the elongated, inclined elliptical shape of  $\rho_{uu}$  seen here is also observed over vegetation canopies in aquatic and terrestrial systems (Yan et al. 2016).

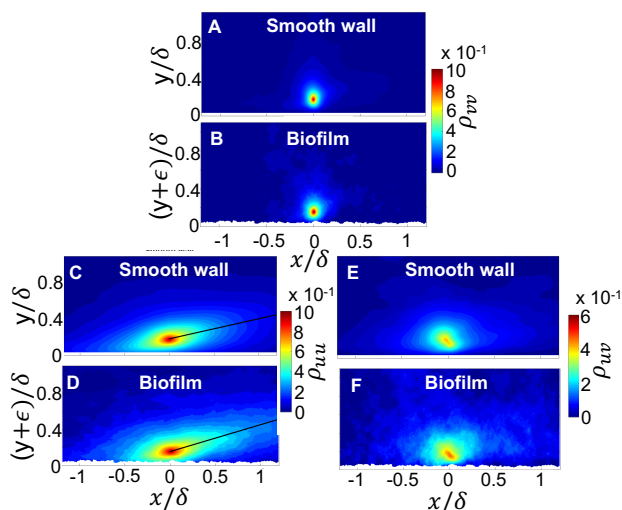


Figure 6. The 2- point correlations,  $\rho_{vv}$  (A & B),  $\rho_{uu}$  (C & D) and  $\rho_{uv}$  (E & F), shown with data from a smooth wall for comparison. The black line in C and D marks the angle of inclination.

The shape of the wall-normal  $\rho_{vv}$  is thought to be indicative of the size of the heads of hairpin packets. As has been shown in studies over other types of roughness, the shape of  $\rho_{vv}$  does not appear affected by the biofilm (Wu and Christensen 2010). The cross correlation  $\rho_{uv}$  also appears similar over the smooth wall and the biofilm. Such similarity in the shape of  $\rho_{uv}$  over a rough and smooth surface was also observed in Volino et al. 2007. This and other studies, however, have shown a reduction in the streamwise length of contours of  $\rho_{vv}$  and  $\rho_{uv}$  with otherwise similar shapes (Wu and Christensen 2010), which is thought to be

due to a decrease in the length scales of large- scale groupings of vortices over rough surfaces.

The angle and spatial extent of these correlations appears to show that the mechanisms of energy and momentum transport in the biofilm flow- hypothesized to be largely due to the presence packets of hairpin vortices that entrain fluid and drive turbulent ejections and sweeps (Wu and Christensen 2010)- is similar in structure to that over the smooth wall. Thus the similarity between the smooth wall and biofilm flows indicates that the structure of the turbulence in the biofilm flow is not substantially different from that over a smooth wall.

## SUMMARY

Though most ship hulls exhibit more sparse, patchy slime fouling, this variability was not address in the present work in order to focus on the interesting flow conditions over a compliant surface. How the generation of turbulence and the structure of that turbulence influences the drag and mass transport on a surface is complex and not easily predicted based on surface characteristics. Turbulent boundary layer measurements were performed over diatomaceous slime-fouled plates using high resolution PIV. The mean velocity profile over the biofilm shows a large downward shift ( $\Delta U^+$ ), resulting in an effective roughness height significantly larger than the physical thickness of the biofilm and generating more than three times as much drag as the smooth-wall. This increase in drag is seen in enhanced  $ke$  and  $RSS$  (Figs. 3 & 4). When normalized by the shear velocity, the  $RSS$  has a similar magnitude, though slightly larger, over the biofilm, but the location of the peak is shifted away from the wall.

Detailed, high resolution measurements of flow above biological surfaces are rare, and the results presented here give important insight into the effects of an algal biofilm at turbulent Reynolds numbers albeit much more modest than observed on a ship. Generally, the mean statistics of the biofilm-fouled surface behaved similarly to a rigid rough wall. Turbulent kinetic energy production appeared dominant at discreet locations along the bed (Fig. 5). Near bed local variability in turbulence production and momentum fluxes indicate that while outer layer similarity is maintained over a biofilm, small scale turbulence structures near the bed, which are important for transport of nutrients to sessile biofilms as well as the hydrodynamic forces that slough biofilm off the surface, are altered by local bed topography created by the biofilm. This dynamic is also observed over coral reefs, where the roughness effects of the reef as a whole determine integrated flow characteristics such as drag coefficient and shear, but at the organismal scale local topography impacts biologically relevant hydrodynamics (Reidenbach et al. 2006). Biofilm growth is highly dependent on fluid motion, even more so than light environment or nutrient concentration (Hondzo and Wang 2002), and it may be that biofilms engineer their near- bed hydrodynamic regime by increasing turbulence in the inner region of the boundary layer.

## REFERENCES

Barros, J. M., Murphy, E. A., and Schultz, M. P., 2016, "Particle Image Velocimetry measurements of the flow over barnacles in a turbulent boundary layer," *18th International Symposium on the Application of Laser and Imaging Techniques to Fluid Mechanics*.

- Castro, I.P., 2007, "Rough-wall boundary layers: mean flow universality," *J. Fluid Mech.*, vol. 585, pp.469-485.
- de Beer, D., and Kühl, M., 2001, "Interfacial microbial mats and biofilms," In: *The benthic boundary layer* (Eds. B. P. Boudreau and B. B. Jørgensen). Oxford University Press, Inc. New York, NY.
- de Beer, D., Stoodley, P., and Lewandowski, Z., 1996, "Liquid flow and mass transport in heterogeneous biofilms," *Water Res.*, vol. 30(11), pp. 2761-2765.
- Flack, K. A., and Schultz, M. P., 2010, "Review of hydraulic roughness scales in the fully rough regime," *J. Fluids Eng.*, vol. 132, pp. 041203.
- Flack, K. A., and Schultz, M. P., 2014, "Roughness effects on wall-bounded turbulent flows," *Phys. Fluids*, vol. 26 pp. 101305
- Flack, K. A., Schultz, M. P., and Shapiro, T. A., 2005, "Experimental support for Townsend's Reynolds number similarity hypothesis on rough walls," *Phys. Fluids*, vol. 17, pp. 035102.
- Graba, M., Moulin, F. Y., Boulêtreau, S., Garabétian, F., Kettab, A., Eiff, O., Sánchez-Pérez, J. M., and Sauvage, S., 2010, "Effect of near-bed turbulence on chronic detachment of epilithic biofilm: Experimental and modeling approaches," *Water Resour. Res.*, vol. 46, pp. W11531.
- Haslbeck, E. G., and Bohlander, G., 1992, "Microbial biofilm effects on drag- lab and field." *Proc. SNAME Ship Production Symp.* Paper No. 3A-1. NAVAL SURFACE WARFARE CENTER CARDEROCK DIV ANNAPOLIS MD
- Hondzo, M., and Wang, H., 2002, "Effects of turbulence on growth and metabolism of periphyton in a laboratory flume," *Water Resour. Res.*, vol. 38, pp. 1277.
- Jimenez, J., 2004, "Turbulent flows over rough walls," *Annu. Rev. Fluid Mech.*, vol. 36, pp.173-196.
- Krogstad, P. Å., and Antonia, R. A., 1999, "Surface roughness effects in turbulent boundary layers," *Exp. Fluids*, vol. 27 pp. 450-460.
- Mejia-Alvarez, R., and Christensen, K. T., 2010, "Low-Order Representations of Irregular Surface Roughness and Their Impact on a Turbulent Boundary Layer," *Phys. Fluids*, vol. 22, pp. 015106.
- Moin, P., and Kim, J., 1985, "The structure of the vorticity field in turbulent channel flow. Part 1: Analysis of instantaneous fields and statistical correlations," *J. Fluid Mech.*, vol. 155 pp. 441-464.
- Molino, P. J., and Wetherbee, R., 2008, "The biology of biofouling diatoms and their role in the development of microbial slimes," *Biofouling*, vol. 24, pp. 365-379.
- Nikora, V. I., Goring, D. G., and Biggs, B. J., 2002, "Some observations of the effects of micro-organisms growing on the bed of an open channel on the turbulence properties," *J. Fluid Mech.*, vol. 450, pp. 317-341.
- Perry, A. E., and Li, J. D., 1990, "Experimental support for the attached-eddy hypothesis in zero-pressure-gradient turbulent boundary layers," *J. Fluid Mech.*, vol. 218, pp. 405-438.
- Reidenbach, M. A., Limm, M., Hondzo, M., and Stacey, M. T., 2010, "Effects of bed roughness on boundary layer mixing and mass flux across the sediment-water interface," *Water Resour. Res.*, vol. 46, pp. W07530.
- Reidenbach, M. A., Monismith, S. G., Koseff, J. R., Yahel, G., and Genin, A., 2006, "Boundary layer turbulence and flow structure over a fringing coral reef," *Limnol. Oceanogr.*, vol. 51, pp. 1956-1968.
- Schultz, M. P., 2007, "Effects of coating roughness and biofouling on ship resistance and powering," *Biofouling*, vol. 23, pp. 331-341.
- Schultz, M. P., and Flack, K. A., 2007, "The rough- wall turbulent boundary layer from the hydraulically smooth to the fully rough regime," *J. Fluid Mech.*, vol. 580, pp. 381-405.
- Schultz, M. P., Bendick, J. A., Holm, E. R., and Hertel, W. M., 2011, "Economic Impact of Biofouling on a Naval Surface Ship," *Biofouling*, vol. 27, pp. 87-98.
- Schultz, M. P., Walker, J. M., Steppe, C. N., and Flack, K. A., 2015, "Impact of diatomaceous biofilms on the frictional drag of fouling-release coatings," *Biofouling*, vol. 31, pp. 759-773.
- Stocking, J. B., Rippe, J. P., and Reidenbach, M. A., 2016, "Structure and dynamics of turbulent boundary layer flow over healthy and algae-covered corals," *Coral Reefs*, vol. 35 pp. 1047-1059.
- Stoodley, P., Lewandowski, Z., Boyle, J. D., and Lappin-Scott, H. M., 1998, "Oscillation characteristics of biofilm streamers in turbulent flowing water as related to drag and pressure drop," *Biotechnol. Bioeng.*, vol. 57 pp. 536-544.
- Stoodley, P., Lewandowski, Z., Boyle, J. D., and Lappin-Scott, H. M., 1999, "Structural deformation of bacterial biofilms caused by short-term fluctuations in fluid shear: An in situ investigation of biofilm rheology," *Biotechnol. Bioeng.*, vol. 65, pp. 83-92.
- Tani, I., 1987, "Turbulent boundary layer development over rough surfaces," In *Perspectives in turbulence studies*, pp. 223-249. Springer Berlin Heidelberg.
- Taherzadah, D., Picioreanu, C., Küttler, U., Simone, A., Wall, W. A., and Horn, H., 2009, "Computational study of the drag and oscillatory movement of biofilm streamers in fast flows," *Biotechnol. Bioeng.*, vol. 105, pp. 600-610.
- Tolhurst, T. J., Consalvey, M., and Paterson, D. M., 2008, "Changes in cohesive sediment properties associated with the growth of a diatom biofilm," *Hydrobiologia*, vol. 596 pp. 225-239.
- Townsin, R.L., 2003, "The ship hull fouling penalty," *Biofouling*, vol. 19 pp. 9-15.
- Volino, R. J., Schultz, M. P., and Flack, K. A., 2007, "Turbulence structure in rough- and smooth-wall boundary layers," *J. Fluid Mech.*, vol. 592, pp. 263-293.
- Volino, R. J., Schultz, M. P., and Flack, K. A., 2009, "Turbulence structure in a boundary layer with two-dimensional roughness," *J. Fluid Mech.*, vol. 635, pp. 75-101.
- Volino, R. J., Schultz, M. P., and Flack, K. A., 2011, "Turbulence structure in boundary layers over periodic two- and three-dimensional roughness," *J. Fluid Mech.*, vol. 676 pp. 172-190.
- Walker, J. M., Flack, K. A., Lust, E. E., Schultz, M. P., and Luznik, L., 2013a, "Experimental and numerical studies of blade roughness and fouling on marine current turbine performance," *Renew. Energ.*, vol. 66 pp. 257-267.
- Walker, J. M., Sargison, J. E., and Henderson, A. D., 2013b, "Turbulent boundary-layer structure of flows over freshwater biofilms," *Exp. Fluids*, vol. 54 pp. 1628.

Wu, Y., and Christensen, K. T., 2007, "Outer-layer similarity in the presence of a practical rough-wall topography," *Phys. Fluids*, vol. 19, pp. 085108.

Wu, Y., and Christensen, K. T., 2010, "Spatial structure of a turbulent boundary layer with irregular surface roughness," *J. Fluid Mech.*, vol. 655, pp. 380-418.

Xu, S., Rempfer, D., and Lumley, J., 2003, "Turbulence over a compliant surface: numerical simulation and analysis," *J. Fluid Mech.*, vol. 478, pp. 11-34.

Yan, C., Nepf, H. M., Huang, W. X., and Cui, G. X., 2016, "Large eddy simulation of flow and scalar transport in a vegetated channel," *Environ. Fluid Mech.*, pp. 1-23.